Pharm Res (2014) 31:969–982
DOI 10.1007/s11095-013-1216-z

RESEARCH PAPER

Classification of the Crystallization Behavior of Amorphous Active Pharmaceutical Ingredients in Aqueous Environments

Bernard Van Eerdenbrugh • Shweta Raina • Yi-Ling Hsieh • Patrick Augustijns • Lynne S. Taylor

Received: 20 May 2013 / Accepted: 18 September 2013 / Published online: 23 November 2013

ABSTRACT

Purpose To classify the crystallization behavior of amorphous active pharmaceutical ingredients (API) exposed to aqueous environments.

Methods A set of approximately 50 chemically and physically diverse active pharmaceutical ingredients (APIs) was selected for this study. Two experimental setups were employed to characterize the crystallization behavior of the amorphous API in an aqueous environment. For the first approach, precipitation, as evidenced by the development of turbidity, was induced using the solvent shift method, by mixing concentrated API solutions in DMSO with an aqueous buffer in a capillary. Subsequently, crystallization was monitored *in situ* over time using synchrotron radiation (simultaneous SAXS/WAXS beamline 12-ID-B at the Advanced Photon Source, Argonne National Laboratories, Argonne, IL). In the second approach, amorphous films were prepared by melt quenching; after adding buffer, crystallization was monitored with time using polarized light microscopy.

Results In general, the crystallization behavior of a given compound was similar irrespective of the experimental method employed. However, the crystallization behavior among different compounds varied significantly, ranging from immediate and complete crystallization to no observable crystallization over biorelevant time scales. Comparison of the observed behavior with previous studies of crystallization tendency in non-aqueous environments revealed that the crystallization tendency of individual APIs was somewhat similar regardless of the crystallization environment.

Conclusions API properties, rather than the method by which amorphous materials are generated, tend to dictate crystallization behavior in aqueous media.

B. Van Eerdenbrugh • S. Raina • Y.-L. Hsieh • L. S. Taylor (✉)
Department of Industrial and Physical Pharmacy, College of Pharmacy
Purdue University, 575 Stadium Mall Drive
West Lafayette, Indiana 47907, USA
e-mail: lstaylor@purdue.edu

B. Van Eerdenbrugh • P. Augustijns
Drug Delivery and Disposition, KU Leuven, Gasthuisberg O&N2
Herestraat 49, Box 921, 3000 Leuven, Belgium

Y.-L. Hsieh
Formulation Sciences, Allergan, Inc., Irvine, California 92612, USA

KEY WORDS active pharmaceutical ingredient · amorphous · crystallization · polarized light microscopy · synchrotron radiation

INTRODUCTION

Currently, drug candidates having low aqueous solubilities tend to dominate developmental pipelines, which can often result in inadequate bioavailability upon oral administration (1). Consequently, there is substantial interest in formulation strategies that lead to bioavailability enhancement. Examples of such formulation strategies include the use of cosolvents (2), complexation using cyclodextrins (3), prodrug strategies (4), particle size reduction (5) and administration of the drug as a disordered amorphous solid (6). Since the amorphous state exhibits a higher energy compared to the crystalline solid, a higher (temporary) concentration relative to the solution concentrations attainable with crystalline solids can be achieved by dissolving the amorphous form. Predictions and experimental determinations have shown that the amorphous form can indeed lead to significant increases in solution concentration, although crystallization of the drug often reduces the amorphous solubility advantage (7–12).

Crystallization of an amorphous active pharmaceutical ingredient (API) can occur during storage as well as upon administration, where the solid is suspended in the fluids present in the intraluminal environment. With respect to solid state stability during storage, previous studies have pointed to the importance of considering the crystallization tendency of the pure amorphous form when evaluating the feasibility of formulating an API as an amorphous solid dispersion (13–16). Therefore, classification methodologies that use small amounts of material have been established to assess the glass forming ability of APIs upon cooling from the melt using differential scanning calorimetry (somewhat analogous with the melt extrusion process, an established unit operation to prepare amorphous solid dispersions) and after rapid solvent evaporation using spin coating (thereby resembling spray-

drying, another standard technique for the preparation of amorphous solid dispersions) (17,18). As such, an API can be classified as being a rapid ('Class I'), intermediate ('Class II') or slow ('Class III') crystallizer (17,18). Although both methodologies and classification criteria differ between the two approaches, it was noted that the crystallization classification of a given compound tended to be somewhat similar, regardless of the approach employed. In other words, API properties, rather than the amorphization methodology applied, appeared to influence crystallization behavior, at least for the preparation methods studied (17,18).

With respect to the crystallization tendency of amorphous APIs in aqueous environments, either from the perspective of an amorphous precipitate formed from a highly supersaturated solution (e.g. that generated upon dissolution of an amorphous solid dispersion, or by a pH change), or with respect to adding amorphous solid (which may crystallize as it dissolves) to an aqueous solution, very little data is available. Crystallization from aqueous environments is obviously an important consideration during delivery of solid amorphous formulations, as well other supersaturating dosage forms. Rapid crystallization will result in a short-lived duration of supersaturation after which absorption will be dictated by the crystalline solubility. In contrast, precipitation to an amorphous form, or maintenance of the amorphous form in an amorphous solid dispersion, will yield supersaturated solutions with enhanced potential for absorption. In a recent study, precipitation of a set of 10 basic drugs was induced using pH change and the desupersaturation profiles as well as the solid state properties of the precipitates formed (crystalline *versus* amorphous) were evaluated (11). It was observed that some compounds crystallized rapidly, resulting in an extremely short duration of supersaturation. In contrast, other compounds precipitated to a disordered form, leading to prolonged supersaturation. Interestingly, there was a certain degree of similarity between the crystallization tendency during the precipitation experiment with the crystallization tendency during and immediately after rapid solvent evaporation.

The aim of the current study was to evaluate the crystallization tendency of APIs in aqueous environments. A set of 51 diverse model compounds was employed, and the crystallization behavior of the compounds was assessed using 2 distinct methodologies. In the first method, precipitation of the APIs was induced using the solvent switch method and crystallinity of the precipitate was monitored over time using synchrotron radiation. In a second approach, API films were prepared by quench melting of crystalline material, exposed to dissolution media; crystallization of the film was probed over time using polarized light microscopy. Subsequently, the crystallization behavior of the APIs was classified as being rapid ('Class I'), intermediate ('Class II') or slow ('Class III'). The crystallization behavior of the various compounds in aqueous media were compared between both methodologies as well as with the behavior observed in the solid state.

MATERIALS AND METHODS

Materials

Benzocaine, dibucaine, lidocaine, miconazole, procaine, and tolbutamide were obtained from Spectrum Chemical (Gardena, CA). Aceclofenac, carvedilol, and loratadine were obtained commercially from Attix Pharmachem (Toronto, ON, Canada). 4-biphenylcarboxylic acid, 4-biphenylmethanol, 4-phenylphenol, acetaminophen, anthranilic acid, benzamide, bifonazole, anhydrous caffeine, chlorpropamide, chlorzoxazone, cinnarizine, clotrimazole, dipyridamole, felbinac (4-biphenylacetic acid), fenofibrate, flufenamic acid, flurbiprofen, haloperidol, indomethacin, indoprofen, ketoprofen, nilutamide, nimesulide, PABA (4-aminobenzoic acid), papaverine HCl, phenacetin (p-acetophenetidide), probucol, tolazamide, tolfenamic acid and 0.5 N hydrochloric acid (HCl) solution were obtained commercially from Sigma-Aldrich, Inc. (St. Louis, MO). Clozapine was purchased from Euroasia (Mumbai, India). Anhydrous theophylline was obtained commercially from Ruger Chemical Co. (Irvington, NJ). Carbamazepine, griseofulvin, itraconazole, ketoconazole, naproxen and piroxicam were obtained commercially from Hawkins, Inc. (Minneapolis, MN). Ibuprofen was purchased from Albemarle Co. (Baton Rouge, LA). Efavirenz and felodipine were obtained commercially from Attix Pharmachem (Toronto, ON, Canada). Loviride was kindly provided by Johnson & Johnson Pharmaceutical Research and Development (Beerse, Belgium). Celecoxib was given by Pfizer, Inc. (Groton, CT). Papaverine free base was prepared from the HCl salt by a method described in the publication by Miyajima *et al.* (19). Carbamazepine dihydrate was prepared from the anhydrate; therefore, 2 g of carbamazepine was added to 50 ml of a 60/40 (v/v) ethanol/water mixture; once carbamazepine was completely dissolved by heating combined with stirring on a hot plate, the mixture was allowed to slowly cool to room temperature, yielding carbamazepine dihydrate overnight; the dihydrate was isolated by filtration and rinsing with water and was stored in a container at 75%RH to prevent dehydration. Dimethyl sulfoxide (DMSO) was obtained from Macron Chemicals (Phillipsburg, NJ). Sodium hydroxide (NaOH) pellets, potassium chloride (KCl), citric acid monohydrate, potassium dihydrogen phosphate (KH_2PO_4), sodium hydrogen carbonate ($NaHCO_3$) and disodium hydrogen phosphate (Na_2HPO_4) were purchased from Mallinckrodt Baker Inc (Phillipsburgh, NJ). D-α-Tocopherol polyethylene glycol 1000 succinate (TPGS) was commercially obtained from Eastman Chemical Company (Kingsport, TN). Yttrium stabilized zirconia beads (diameter

0.5 mm, YTZ grinding media) were purchased from Tosoh Corporation Advanced Ceramics Department (Tokyo, Japan). All buffers were prepared in deionized water.

Buffer Selection and Preparation

For the different APIs, buffers were selected to maximize the relative contribution of the unionized species in the solution phase. Therefore, the pKa's of the different APIs were calculated with ChemAxon's pKa calculator plugin using MarvinSketch 5.11.5 (ChemAxon Kft., Budapest, Hungary). pKa's were calculated within the range of −10 to +20 at 298 K and all default values of the plugin were used for the calculations. To minimize the relative contribution of ionized species, each buffer pH was selected in the pKa region where the unionized species showed its maximum and, when possible, at least 2 units from the nearest pKa value(s). The regions where the unionized species show their maximum, the pH value selected for each buffer and the melting points of the different model compounds are summarized in Table I. For buffer preparation, solutions of KCl (pH 1 and 1.6), citric acid (pH 3.6 and 5), KH_2PO_4 (pH 7 and 8), $NaHCO_3$ (pH 10) and Na_2HPO_4 (pH 11 and 12) were prepared so that 0.2 M solutions were obtained upon reaching the total volume of the volumetric flasks. To these solutions, water and either a 0.5 N solution of HCl (for buffers of pH 1, 1.6 and 3.6) or a 1 N solution NaOH (for buffers of pH 5, 7, 8, 10, 11 and 12) were added so that the target pH was met upon reaching the total desired buffer volume.

Synchrotron Experiments: Crystallization Behavior of Precipitates Created From Highly Supersaturated Solutions

X-ray diffraction (XRD) experiments were conducted at the Advanced Photon Source beam station 12-ID-B [simultaneous Small-Angle X-ray Scattering/Wide-Angle X-ray Scattering (SAXS/WAXS) instrument, Argonne National Laboratories, Argonne, IL]. An overview of the beamline setup is provided in Fig. 1a, showing the direction of the X-ray beam (orange arrow) and the location of the sample holder, SAXS and WAXS detectors. As the SAXS data collected was not used for this study, further description and figure panels will be limited to the WAXS capabilities of the instrument. The instrument was equipped with a Pilatus 300 K WAXS detector (Dectris Ltd., Baden, Switzerland). The energy of the X-ray source was 12 keV ($\lambda = 1.033$ Å), and the sample to detector distance was 455 mm. The Q range probed was 0.88–2.44 $Å^{-1}$. Q ranges were calibrated using silver behenate and the absolute intensity was calibrated using glassy carbon. The exposure time used for each measurement was 1 s.

Table I pH Region of Maximal Fraction of Unionized Species, pH of the Selected Buffer and Relevant Properties of the Model APIs

API	pH region of unionized species[a]	pH	MW[b]	T_m[b]
4-biphenylcarboxylic acid	pH < 4.07	1.0	198	227
4-biphenylmethanol	pH < 15.00	7.0	184	100
4-phenylphenol	pH < 9.89	7.0	170	166
Aceclofenac	−2.08 < pH < 3.44	1.0	354	153
Acetaminophen	pH < 9.46	7.0	151	170
Anthranilic acid	1.95 < pH < 4.89	3.6[c]	137	147
Benzamide	−1.24 < pH < 14.56	7.0	121	127
Benzocaine	pH > 2.78	7.0	165	89
Bifonazole	pH > 6.69	11.0	310	151
Caffeine	pH > −0.92	7.0	194	237
Carbamazepine	−3.75 < pH < 15.96	7.0	236	192
Carvedilol	8.94 < pH < 14.09	11.0	408	117
Celecoxib	−0.42 < pH < 10.70	7.0	381	163
Chlorpropamide	pH < 4.33	1.0	277	124
Chlorzoxazone	pH < 9.39	5.0	170	191
Cinnarizine	pH > 8.40	12.0	369	121
Clotrimazole	pH > 6.62	11.0	345	145
Clozapine	7.36 < pH < 16.65	10.0	327	185
Dibucaine	9.04 < pH < 14.57	12.0	343	65
Dipyridamole	6.59 < pH < 14.97	11.0	505	164
Efavirenz	pH < 12.52	7.0	316	139
Felbinac	pH < 4.71	1.0	212	164
Felodipine	pH > 3.72	7.0	384	147
Fenofibrate	pH > −4.93	7.0	361	81
Flufenamic acid	−2.14 < pH < 3.88	1.0	281	135
Flurbiprofen	pH < 4.42	1.0	244	115
Griseofulvin	−4.32 < pH < 17.69	7.0	353	218
Haloperidol	8.05 < pH < 13.96	11.0	376	152
Ibuprofen	pH < 4.85	1.0	206	77
Indomethacin	pH < 3.80	1.0	358	161
Indoprofen	pH < 4.44	1.0	281	212
Itraconazole	pH > 3.92	7.0	706	168
Ketoconazole	pH > 6.75	11.0	531	150
Ketoprofen	pH < 3.88	1.0	254	95
Lidocaine	7.75 < pH < 13.78	11.0	234	68
Loratadine	pH > 4.33	11.0	383	136
Loviride	pH < 11.57	7.0	372	227
Miconazole	pH > 6.77	11.0	417	86
Naproxen	pH < 4.19	1.0	230	162
Nilutamide	pH < 15.01	7.0	317	155
Nimesulide	pH < 6.86	1.0	308	150
PABA	2.69 < pH < 4.77	3.6[c]	137	189
Papaverine	pH > 6.03	10.0	339	148
Phenacetin	pH < 14.98	7.0	179	136
Piroxicam	1.01 < pH < 2.27	1.6[c]	331	203
Probucol	pH < 10.29	7.0	517	127
Procaine	pH > 8.96	12.0	236	62

Table I (continued)

API	pH region of unionized species[a]	pH	MW[b]	T_m[b]
Theophylline	$-0.78 < pH < 7.82$	5.0	180	272
Tolazamide	$1.61 < pH < 4.07$	3.6[c]	311	172
Tolbutamide	$pH < 4.33$	1.0	270	129
Tolfenamic acid	$-2.10 < pH < 3.88$	1.0	262	213

[a] Values provided are the calculated pKa values

[b] Values were taken from references (11,17). If values could not be found in these references, ChemAxon's Elemental Analysis calculator plugin was used (for MW) or the methodology described in (17) was used (for T_m)

[c] Partly ionized and/or zwitterionic

Suspensions of the APIs were created using the solvent shift method, i.e. by mixing a concentrated DMSO solution of the drug with buffer. A standard concentration of 100 mg/ml was used for the DMSO solutions, although in a number of cases a lower (due to too low a solubility in DMSO; bifonazole 40 mg/ml, caffeine 40 mg/ml, cinnarizine 20 mg/ml, clotrimazole 40 mg/ml, haloperidol 40 mg/ml, ketoconazole 20 mg/ml, loviride 40 mg/ml, probucol 40 mg/ml, and theophylline 40 mg/ml) or higher concentration (due to too high a solubility in aqueous media; acetaminophen 500 mg/ml, benzamide 500 mg/ml) was applied.

Two different setups were used to examine crystallization behavior in an aqueous environment, one to evaluate short term crystallization behavior and one to probe long term crystallization behavior. A simplified schematic of the setup used for the evaluation of short term crystallization behavior can be found in Fig. 1b. The setup consisted of a peristaltic pump (red rectangle, a Masterflex® console equipped with a Masterflex® Easy-Load® II pump head, Cole-Parmer, Vernon Hills, IL) used to transfer the buffer (light blue) through flexible tubing (dark grey, Cole-Parmer, Vernon Hills, IL) to a DMSO solution of API at the bottom of a capillary (dark blue, Mettler ME 18552, Mettler Toldeo, Columbus, OH), where a drug precipitate was formed. The nature of the precipitate was probed by directing the synchrotron X-ray beam (thick orange arrow) through the suspended material and recording scattered and/or diffracted X-rays (thin orange arrow) on the WAXS detector (orange rectangle). Figure 1c provides a picture of the sample environment for these experiments showing the capillary connected to the tubing and the direction of the X-ray beam (orange arrow). For these short term experiments, it was desirable to determine crystallization behavior *in situ*, immediately after precipitation of the API. This was achieved as shown in the schematic

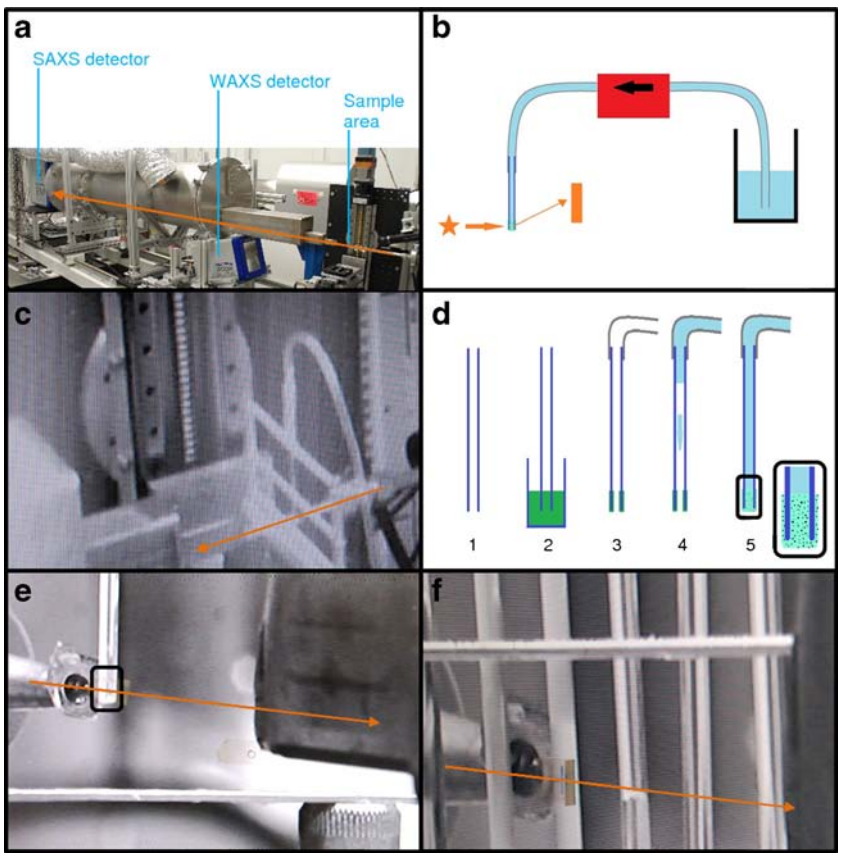

Fig. 1 Setup for the synchrotron experiments. See text for further detail on the different panels. (**a**) Overview of the 12-ID-B beam line setup. (**b**) Simplified schematic of the setup used for the evaluation of short term crystallization behavior. (**c**) Details of the setup used for the study of short term crystallization behavior (**d**) Schematic illustrating the different steps of formation of a precipitate at the bottom of the capillary. (**e**) Details of the visual examination of precipitate formed upon mixing of the API solution in DMSO with the buffer. (**f**) Sample holder used for the examination of long term crystallization behavior.

provided in Fig. 1d, which illustrates the different steps involved in forming a precipitate at the bottom of the capillary. First, the empty capillary (d1, dark blue) was gently dipped into an API solution in DMSO (d2, dark green), leaving a film on the capillary (d3, dark green). Subsequently, the capillary was connected to the tubing (d3, dark grey) and buffer was guided through the tubing towards the DMSO film (d4, light blue). Upon making contact with the film, the flow of the buffer was halted, the two liquids mixed spontaneously (d5, light green) and a precipitate formed (d5, black dots). As the peristaltic pump could be halted from outside the experimental hutch, the precipitate could be probed as it formed. Formation of the precipitate could be visually examined as it gives rise to turbidity, as shown in Fig. 1e, where the turbidity observed within the black rectangle clearly points to precipitation and the formation of a suspension that can be probed by X-rays (orange arrow). For these short term experiments, measurements were conducted for 150 s, whereby between each consecutive 1 s measurement a dead time of about 400 μs occurred. Each experiment was performed in duplicate.

For long term crystallization behavior, a simpler approach was used. Briefly, 100 μl of DMSO stock solution was added to a 1.5 ml Eppendorf tube (Eppendorf, Hamburg, Germany) containing 900 μl of buffer. Again, upon mixing of the liquids by shaking the tube, a turbid suspension formed which was transferred into a capillary (Mettler ME 18552, Mettler Toldeo, Columbus, OH). Subsequently both ends of the capillary were sealed off with wax (to prevent leakage and evaporation over time). Samples were placed into a multi-sample holder (Fig. 1f) and samples were measured after 15 min, 30 min, 1 h and 24 h. Two separate measurements were performed at each time point, by probing different regions of the capillary.

To obtain reference data and to evaluate the lower limit at which crystallinity can be detected in the samples, measurements were taken of the pure crystalline APIs as well as of a dilution series (twofold dilutions in water) of a nanosuspension of loviride stabilized by TPGS [100% (w/w), relative to the drug weight]. In cases where the grain size of the crystalline API reference powder was too large (resulting in isolated intense spots rather than circular features on the 2D detector), powders were subjected to milling using a mortar and pestle, in order to obtain better quality diffractograms. The nanosuspension was prepared by media milling 1 g of API for 24 h using a ball mill, as described in detail elsewhere (20). The nanosuspension had a Z-average particle diameter of 151 ± 1 nm and a polydispersity index of 0.142 ± 0.011, as determined by dynamic light scattering [see (21) for details on the procedure]. For the synchrotron experiments, crystalline references were measured once, nanosuspensions were measured in triplicate and averages and standard deviations were calculated. All measurements were performed in capillaries (Mettler ME 18552, Mettler Toldeo, Columbus, OH, length 30.4 mm, outer diameter: 1 mm, inner diameter: 0.7–0.8 mm). To quantify peak intensity of the most intense peak of the loviride nanosuspensions (1.81–1.82 $Å^{-1}$) as a function of loviride content, the average of the minima at both sides of the peak (1.77–1.78 $Å^{-1}$ and 1.87–1.89 $Å^{-1}$) was subtracted from the peak maximum (1.81–1.82 $Å^{-1}$).

Polarized Light Microscopy Experiments: Crystallization Behavior of Hydrated Amorphous Films Prepared Using Melt Quenching

For the evaluation of crystallization tendency using polarized light microscopy (PLM), samples were prepared by melting the APIs in a small vessel, constructed from alumina foil, on a hot plate. Subsequently, a circular cover slip (18 mm diameter, VWR, Radnor, PA) was brought into contact with the top of the melt and quickly removed. As such, a film of material was deposited on the cover slip, which quickly solidified upon removal from the heat source. These solidified films, with their API side facing upward, were then transferred into a 12 well plate (353043, BD Falcon™, San Jose, CA), prefilled with 4 ml buffer. Crystallization behavior of the films in the wells was evaluated over time with PLM using an Eclipse E600 POL polarizing microscope (Nikon Corporation, Tokyo, Japan), equipped with 4×,10×,20×, and 40× objectives. Crystallinity was evaluated visually, based on the observed birefringence throughout the film. This two-dimensional analysis enables a semi-quantitative evaluation of crystallinity based on the relative areas of crystalline (birefringent) and amorphous (non-birefringent) regions. As such, an overall crystallinity value between 0% and 100% was assigned to each sample, using 10% increments. This was done for each sample after 5 min, 10 min, 15 min, 30 min, 1 h, and 24 h.

RESULTS AND DISCUSSION

Crystallization Behavior of Precipitates Created from Highly Supersaturated Solutions

In this approach, precipitates were formed by creating highly supersaturated solutions by the mixing of an API solution in DMSO and buffer. This approach, sometimes referred to as the solvent switch method, is frequently used to evaluate the impact of additives on the precipitation behavior of APIs (e.g. 22–24). It is also represents a situation where a highly supersaturated solution of a drug is rapidly formed e.g. following a pH change or the fast dissolution of an amorphous solid dispersion under non-sink conditions. In these situations, it is highly likely that a precipitate will be formed (11,22–25). However, it is important to characterize the resultant precipitate, since the extent of supersaturation remaining in solution is correlated to the form that phase separates; solutions which

precipitate to metastable forms will still be supersaturated with respect to the most stable crystal form. It has been observed that the solvent switch method has a high probability of inducing liquid-liquid phase separation (11,12,26) as a precursor to crystallization, yielding an initially amorphous precipitate, which might take the form of colloidal species. Since all of the compounds evaluated in this study tend to be poorly water soluble, dilution of the DMSO solution with buffer will generate very high supersaturations, leading to a precipitate in all cases. Using the capillary method described above, and a 100 mg/ml solution of drug in DMSO (the standard concentration used for these experiments) it can be estimated, based on the weight gain obtained after dipping the capillary into the aqueous solution, that the resulting amount of total drug (dissolved and precipitated) will be around 10 mg/ml. Therefore, the first evaluation that needed to be performed was to determine if crystallinity can be picked up at these precipitate concentrations using synchrotron radiation.

As a first test, a dilution series of loviride nanosuspensions was measured. As can be seen from Fig. 2a, the diffractogram of the loviride nanosuspension consists of a diffuse scattering halo arising from water on which the crystalline diffraction peaks of loviride are superimposed. Note that the small peaks at 1.39, 1.85 and 1.89 $Å^{-1}$ in the blank are artifacts. Evaluation of the most intense diffraction peak at 1.81–1.82 $Å^{-1}$ as a function of loviride content (Fig. 2b–c), suggests that crystallinity can be detected down to suspension concentrations of 2.6 mg/ml, while upon further dilution to 1.3 mg/ml, the signal tends to be lost within the noise of the measurement. This trend can be seen more clearly by plotting the peak height of this peak as a function of loviride content. Over the complete range of suspension concentrations (Fig. 2d), as well as at lower concentrations (Fig. 2e), a linear relationship is obtained with a correlation coefficient above 0.99. However, it can be seen that the standard deviations at 2.61 and 1.30 mg/ml start to overlap, suggesting that the detection of crystallinity becomes challenging at these suspension concentrations. The fact that good linearity can be observed for these dilution series is related to the small particle size of the nanosuspensions. Hence good statistics can be obtained for every measurement, as can be seen from the nice circular features in the raw data of a 167 mg/ml suspension (Fig. 2f). To obtain further insight into the lowest detectable levels of crystallinity in precipitates of the other APIs, the height of the 1.81–1.82 $Å^{-1}$ peak in the diffractogram of pure crystalline loviride reference was compared to that of the highest peak found in the diffractograms of the pure crystalline references of the other APIs. The resulting ratios are provided in Table II. As can be seen from Table II, virtually all of the APIs have ratios higher than 1. Although the approach taken here is not fully quantitative, it suggests that for the vast majority of the compounds evaluated, the lowest concentration detectable will be lower than for loviride and thus that the synchrotron based technique is applicable to assess the crystallization behavior of the precipitated material.

To classify the crystallization behavior of the different compounds, the following criteria were used: a compound showing diffraction peaks within the short term experiments (150 s) was classified as a Class I compound or a rapid crystallizer. For a Class II compound or an intermediate crystallizer this could not be observed, although crystallinity could be observed after 1 h. Compounds requiring longer crystallization times were classified as Class III compounds or slow crystallizers. Representative results for carbamazepine, a compound that shows Class I crystallization behavior, are provided in Fig. 3. Figure 3a provides the data obtained for carbamazepine anhydrate [Form III (27) upper part, black curve] and dihydrate (upper part, red curve) and the short timescale kinetic data obtained (lower part). From the kinetic data, four distinct phases can be distinguished. Initially, an amorphous halo can be observed that remains unchanged during the first 9 s of the experiments. This arises from the concentrated DMSO solution of carbamazepine prior to mixing with buffer. Subsequently, buffer reaches the DMSO solution and mixing occurs (9–13 s), giving rise to significant changes in the form of the amorphous halo. Third, an amorphous phase can be observed that remains unchanged for about 40 s (13–55 s). Finally, after 55 s, (46 s after mixing between DMSO and buffer commenced), diffraction peaks show up, clearly showing the appearance of crystalline carbamazepine. As carbamazepine has the ability to crystallize into different forms, it is of interest to further evaluate the diffraction peaks in more detail. Based on Fig. 3b–e, it is clear that the crystalline material formed corresponds to the dihydrate of carbamazepine. Furthermore, it is of interest to observe that the intensities of the peaks vary as a function of time and, in general (with the exception of the peaks between 1.70 and 1.72 $Å^{-1}$), tend to do so independently from each other. This is a result of the fact that a particle needs to have the proper orientation relative to the incoming X-rays in order to give rise to a Bragg peak. The data from later time points confirmed the formation of carbamazepine dihydrate (data not shown).

An example of a compound showing an intermediate or Class II crystallization tendency is flufenamic acid, for which relevant diffractograms are provided in Fig. 4. As can be seen from the figure, no crystallinity can be observed at the end of the short term experiment (150 s). In contrast, at later time points (15 min, 30 min and 1 h), clear diffraction peaks can be observed. The location of the Bragg peaks did not correspond to those of the crystalline reference, which is the thermodynamically stable form at room temperature [Form III, (28,29)]. Rather, upon careful evaluation of powder diffractograms computed from the crystal structures of flufenamic acid polymorphs found in the Cambridge Structural Database (30), it could be concluded that the structure corresponds to Form I of

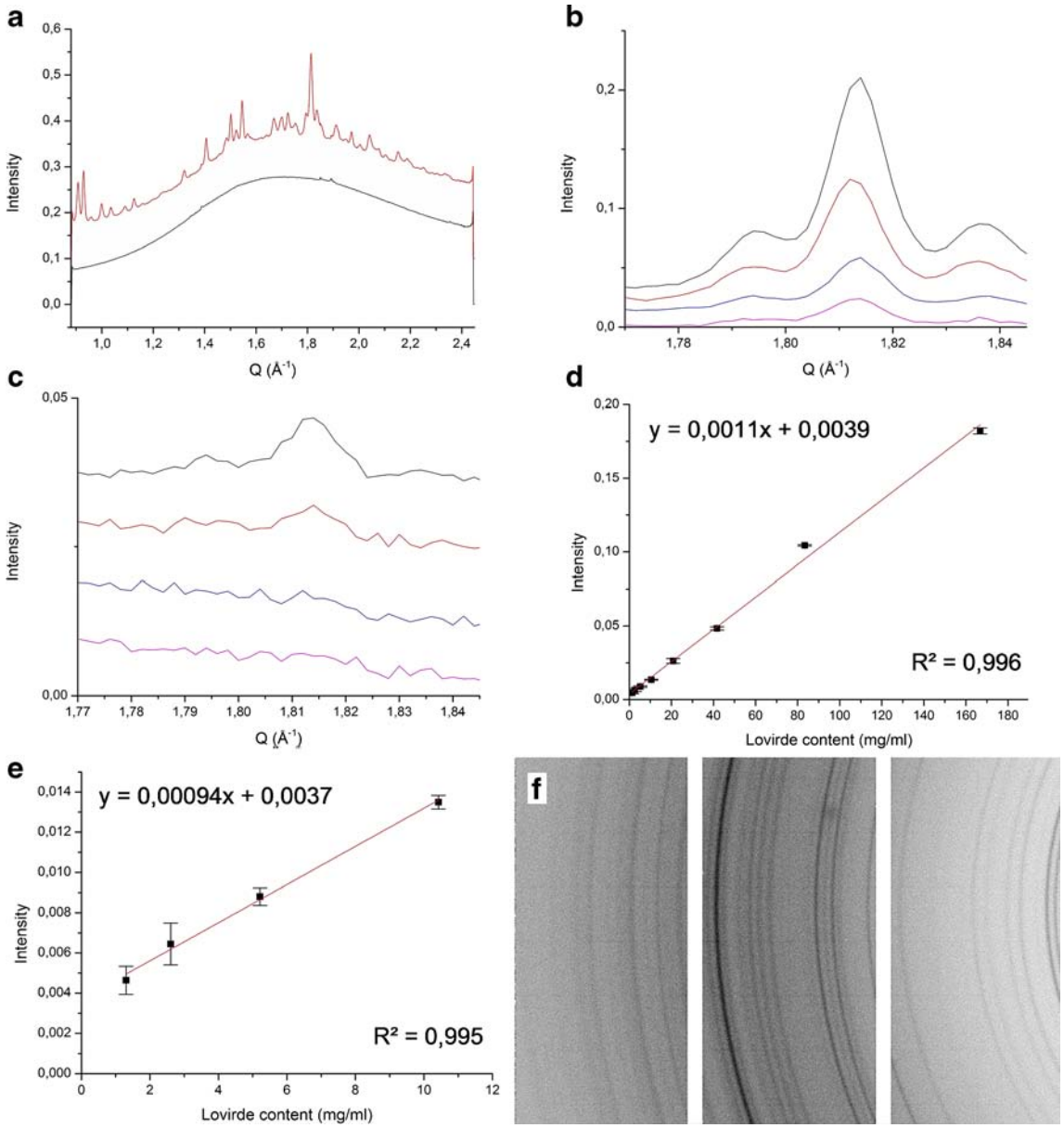

Fig. 2 Measurements on loviride nanosuspensions. (**a**) Diffractogram of a blank solution (*black*) and a 167 mg/ml loviride nanosuspension (*red*, *curve* was offset by 0.1 units). (**b**) Intensity of the loviride peak at 1.81–1.82 $Å^{-1}$ as a function of loviride content: 167 mg/ml (*black*), 83.4 mg/ml (*red*), 41.7 mg/ml (*blue*) and 20.9 mg/ml (*purple*). Diffractograms were offset. (**c**) Intensity of the loviride peak at 1.81–1.82 $Å^{-1}$ as a function of loviride content: 10.4 mg/ml (*black*), 5.21 mg/ml (*red*), 2.61 mg/ml (*blue*) and 1.30 mg/ml (*purple*). Diffractograms were offset. (**d**) Linearity of the 1.81–1.82 $Å^{-1}$ peak as a function of loviride content: 167–1.30 mg/ml range. (**e**) Linearity of the 1.81–1.82 $Å^{-1}$ peak as a function of loviride content: 10.4–1.30 mg/ml range. (**f**) Raw WAXS data of a 167 mg/ml loviride nanosuspension.

flufenamic acid (CSD-FPAMCA11), which is enantiotropically related to Form III (CSD-FPAMCA) with a transition temperature of 42°C (28,31,32). Finally, ketoconazole serves as an example of a compound for which slow crystallization behavior (Class III) was observed (Fig. 5). In this case, no crystallization could be seen, even after 1 h of monitoring. Only after 24 h, could the characteristic diffraction peaks of ketoconazole be observed.

The crystallization behavior of the precipitates formed from all of the model APIs with the solvent shift method is summarized in Table III. In total, the crystallization tendency of 47 compounds could be classified using this method [4 compounds (benzocaine, PABA, papaverine and theophylline) were excluded due to the inability to induce precipitation and/or the data obtained being inconclusive]. As can be seen from Table III, the compounds tend to be fairly evenly distributed among the three different crystallization classes, with 15 Class I (32%, fast crystallizers), 17 Class II (36%, intermediate crystallizers) and 15 Class III (32%, slow crystallizers) compounds.

Table II Ratios Between the Maximum Peak Intensity in the Diffractogram of the Crystalline API and the 1.81–1.82 $Å^{-1}$ Peak in the Diffractogram of Pure Crystalline Loviride

API	Ratio	API	Ratio	API	Ratio
4-biphenylcarboxylic acid	4.9	Clozapine	6.6	Lidocaine	3.3
4-biphenylmethanol	1.6	Dibucaine	2.1	Loratadine	0.9
4-phenylphenol	10.8	Dipyridamole	1.9	Miconazole	0.7
Aceclofenac	3.0	Efavirenz	1.0	Naproxen	2.0
Acetaminophen	2.3	Felbinac	3.0	Nilutamide	1.9
Anthranilic acid	1.6	Felodipine	3.2	Nimesulide	1.1
Benzamide	3.1	Fenofibrate	6.7	PABA	3.3
Benzocaine	2.1	Flufenamic acid	2.8	Papaverine	1.4
Bifonazole	2.8	Flurbiprofen	1.8	Phenacetin	3.8
Caffeine	1.7	Griseofulvin	1.5	Piroxicam	6.0
Carbamazepine	4.4	Haloperidol	4.6	Probucol	6.4
Carvedilol	1.5	Ibuprofen	6.4	Procaine	7.3
Celecoxib	1.4	Indomethacin	5.7	Theophylline	1.2
Chlorpropamide	2.9	Indoprofen	1.9	Tolazamide	1.3
Chlorzoxazone	14.8	Itraconazole	1.0	Tolbutamide	22.0
Cinnarizine	8.8	Ketoconazole	1.6	Tolfenamic acid	2.6
Clotrimazole	3.0	Ketoprofen	1.1		

It might be expected that the observed variations in crystallization rate can be explained by differences in the extent of supersaturation achieved for the various compounds. According to classical nucleation theory, the extent of supersaturation is a major factor in determining the nucleation rate (33). The supersaturation is typically estimated from the ratio of the solution concentration generated to the equilibrium solubility of the stable crystalline form. Since the initial concentration generated was constant, the variation in supersaturation for the various compounds depends on differences in their crystal solubility. However, despite the supersaturation providing the thermodynamic driving force for nucleation, no correlation was seen between the crystallization tendency and the solubility of the various compounds tested. For example, itraconazole has extremely low aqueous solubility (an estimated solubility of about 1 ng/mL has been reported at neutral pH) (34), and therefore is extremely supersaturated in these experiments, yet fails to crystallize. In contrast, benzamide, lidocaine and caffeine have much higher aqueous solubilities [with reported solubility values at 25°C of 13.40 mg/mL (benzamide), 3.820 mg/mL (lidocaine), and 19.42 to 21.46 mg:mL (caffeine)] (35), and therefore are comparably less supersaturated, yet crystallize readily. Thus no trends can be seen between aqueous solubility/degree of supersaturation and crystallization tendency.

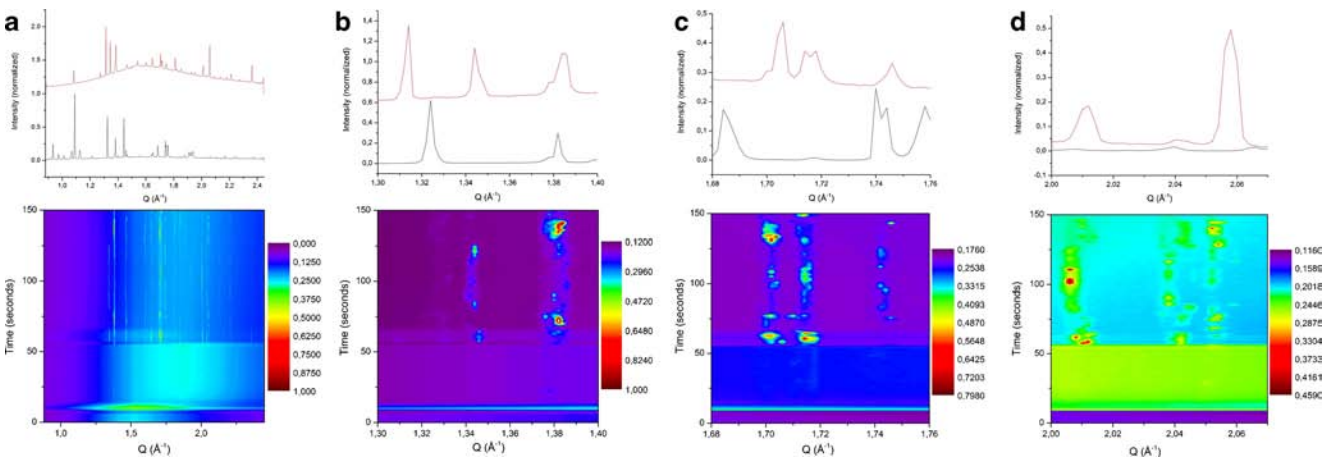

Fig. 3 Short term crystallization behavior of carbamazepine. Reference diffractograms are those of carbamazepine anhydrate (*black curve*) and carbamazepine dihydrate (*red curve*). (**a**) Complete WAXS region (0.88–2.45 Å), (**b**) 1.30–1.40 $Å^{-1}$ range, (**c**) 1.68–1.76 $Å^{-1}$ range, and (**d**) 2.00–2.07 $Å^{-1}$ range.

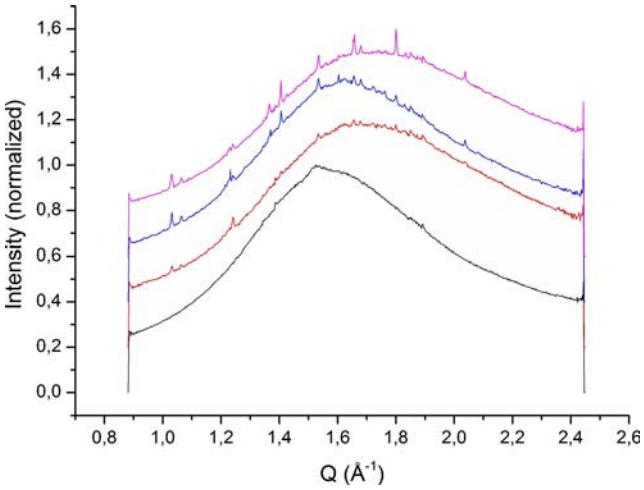

Fig. 4 Crystallization behavior of flufenamic acid. Key: diffractogram at the end of the short term experiment (150 s, *black*), after 15 min (*red*), after 30 min (*blue*) and 1 h (*purple*). Diffractograms were offset.

Crystallization Behavior of Hydrated Amorphous Films Prepared Using Melt Quenching and Comparison of Crystallization Behavior in Different Environments

As a complementary technique, polarized light microscopy (PLM) was used to evaluate crystallization tendency of melt quenched amorphous films exposed to buffer. It is well known that amorphous solids can crystallize during dissolution, both as they become hydrated and when they generate supersaturated solutions (7,32,36). The crystallization tendency from amorphous solids is of practical relevance, e.g. in the instance when experimental determination of amorphous solubility is being attempted, or for amorphous suspension formulations. For these experiments,

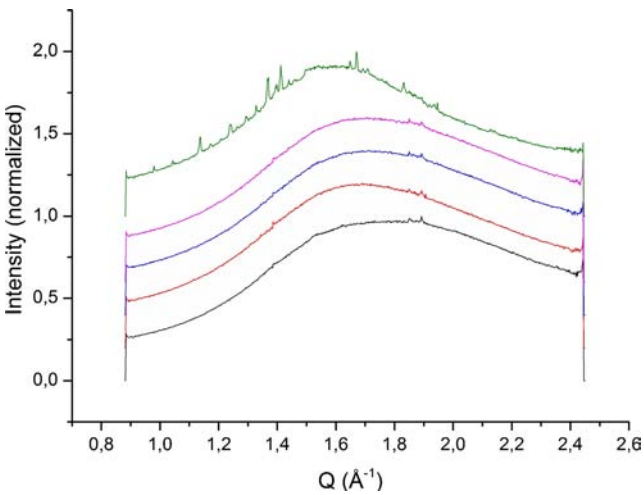

Fig. 5 Crystallization behavior of ketoconazole. Key: diffractogram at the end of the short term experiment (150 s, *black*), after 15 min (*red*), after 30 min (*blue*), 1 h (*purple*) and 24 h (*green*). Diffractograms were offset.

Table III Classification Results Using the Solvent Shift Method

	Class I	Class II	Class III
	4-biphenylcarboxylic acid	Aceclofenac	Bifonazole
	4-biphenylmethanol	Acetaminophen	Carvedilol
	4-phenylphenol	Anthranilic acid	Cinnarizine
	Benzamide	Celecoxib	Clotrimazole
	Caffeine	Chlorpropamide	Clozapine
	Carbamazepine	Chlorzoxazone	Efavirenz
	Felbinac	Dibucaine	Ibuprofen
	Indoprofen	Dipyridamole	Indomethacin
	Lidocaine	Felodipine	Itraconazole
	Loviride	Fenofibrate	Ketoconazole
	Naproxen	Flufenamic acid	Ketoprofen
	Phenacetin	Flurbiprofen	Loratadine
	Piroxicam	Griseofulvin	Miconazole
	Tolazamide	Haloperidol	Probucol
	Tolfenamic acid	Nilutamide	Procaine
		Nimesulide	
		Tolbutamide	
Total	15	17	15
Percentage	32	36	32

the criteria to classify crystallization behavior were set as follows: a Class I compound was a compound for which all of the solid material of the film was birefringent within 5 min, Class II compounds were completely birefringent within 1 h whereas for Class III compounds a completely birefringent film could not be observed within 1 h.

Figure 6 provides examples of model compounds falling into each of the three classes based on this methodology. For flurbiprofen (Fig. 6a), a completely birefringent image can be observed 5 min after submerging the amorphous film in the buffer, thereby serving as an example of a Class I compound. For fenofibrate, isolated crystals in an amorphous film can be observed after 30 min (Fig. 6b) which evolves into a completely crystalline film within an hour (Fig. 6c), thereby showing Class II behavior. Finally, ketoprofen serves as an example of a Class III compound. Clearly, crystallization is not complete for this compound after 1 h (Fig. 6d). After 24 h however, this compound crystallized completely (data not shown).

The type of classification illustrated above could be performed for all model compounds; a general overview of the classification results obtained for all of the compounds evaluated using this method is provided in Table IV. Class I compounds tend to be the most dominant class for this classification system, representing 26 out of 50 compounds (52%). Only 8 compounds (16%) are classified as Class II compounds while 16 compounds (32%) were classified as Class III compounds. As such, it seems that using this evaluation system,

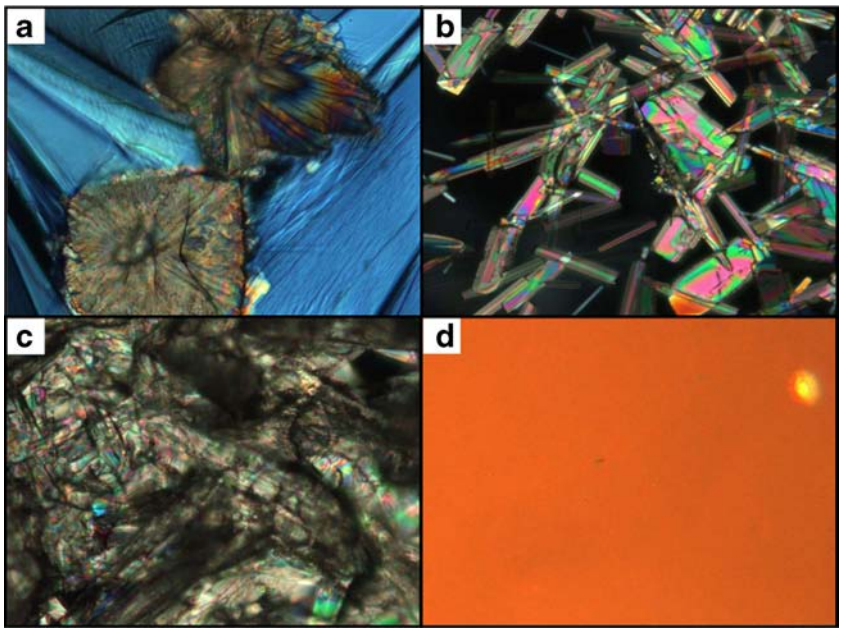

Fig. 6 Representative PLM micrographs for classification using the melt quench method. (**a**) flurbiprofen subjected to buffer for 5 min, (**b**) fenofibrate subjected to buffer for 30 min, (**c**) fenofibrate subjected to buffer for 1 h, and (**d**) ketoprofen subjected to buffer for 1 h. Size of all images is 500 μm × 375 μm.

Table IV Classification Results Using the Melt Quench Method

	Class I	Class II	Class III
	4-biphenylcarboxylic acid	Chlorpropamide	Aceclofenac
	4-biphenylmethanol	Fenofibrate	Bifonazole
	4-phenylphenol	Griseofulvin	Carvedilol
	Acetaminophen	Ibuprofen	Celecoxib
	Anthranilic acid	Loviride	Cinnarizine
	Benzamide	Nimesulide	Clotrimazole
	Benzocaine	Piroxicam	Clozapine
	Caffeine	Procaine	Efavirenz
	Carbamazepine		Felodipine
	Chlorzoxazone		Indomethacin
	Dibucaine		Ketoconazole
	Dipyridamole		Ketoprofen
	Felbinac		Loratadine
	Flufenamic acid		Miconazole
	Flurbiprofen		Probucol
	Haloperidol		Tolazamide
	Indoprofen		
	Lidocaine		
	Naproxen		
	Nilutamide		
	PABA		
	Papaverine		
	Phenacetin		
	Theophylline		
	Tolbutamide		
	Tolfenamic Acid		
Total	26	8	16
Percentage	52	16	32

more compounds were classified as Class I compound at the expense of Class II compounds.

It is of interest to compare the observed crystallization behavior for the two different approaches. With respect to this, it should be noted that there are subtle differences between the methods. First, the classification criteria used differ slightly: whereas a cut-off value of 2.5 min was used to distinguish a Class I from a Class II compound in the synchrotron experiments, for experimental reasons, a value of 5 min was used in the experiments where polarized light microscopy was used. This difference in cut-off time may explain why more Class I compounds were seen with the melt quenched films. Second, it should be noted that there is a difference in the manner in how crystallinity is evaluated: for the synchrotron experiments, crystallinity means that crystallinity can be observed in the diffratograms. This does not necessarily mean that the sample has completely crystallized at this point. For the experiments where PLM was used, a sample is classified as crystalline at a certain time point only if birefringence can be observed throughout the complete film. Third, and finally, there is a difference in the crystallization environment and the nature of the amorphous solids formed: for the synchrotron experiments, where the solids were prepared by a solvent shift, the amorphous matrix that is precipitated can be expected to be fully hydrated, as it is formed in an aqueous environment. When melt quenching is applied, water can be expected to be absent initially, as the heat applied will cause any water present to be removed from the sample. Subsequently, upon exposure to buffer, water will gradually hydrate the sample, starting from the surface and penetrating into the sample. These differences in hydration may be important since the presence or absence of water in the amorphous matrix will

influence mobility, which may in turn influence crystallization behavior. In addition, the extent of supersaturation that can be generated in the amorphous films is much lower than that created by the solvent switch experiments, a factor which might be expected to reduce crystallization tendency. However, other factors that favor crystallization are present for these samples, in particular the fact that the amorphous films provide a surface for heterogeneous nucleation. Despite the afore-mentioned differences, it is apparent from a comparison between the methods (Table Va (left)) that the crystallization behavior of the compounds is rather similar. Furthermore, the dominant cause for differences seen in classification behavior arises from the classification of a compound as an intermediate crystallizer using the solvent switch method, and as a Class I compound with the melt quench method (22%). Further analysis presented in Table V (right column) reveals that 61% of the compounds are classified identically, 37% are classified slightly different (i.e. one methodology places the compound as an intermediate crystallizer while the other approach classifies the compound as showing Class I or Class III behavior), and only in 2% of the cases is an extremely different classification result obtained (this was for tolazamide, a rapid crystallizer according to the melt quench method and a Class III molecule according to the solvent shift method). In addition, it is also of interest to evaluate to what extent crystallization behavior in an aqueous environment is similar to that seen in the solid state. In the context of amorphous formulations, understanding the tendency for crystallization in both the solid state and from solution is critical for determining failure mechanisms as well as for understanding the likely extent of bioavailability enhancement. In terms of solid state stability, the amorphous formulation needs to remain amorphous for the shelf life of the product. If crystallization occurs, then the formulation will not lead to a supersaturated solution. Likewise, if solid state stability can be maintained, but the supersaturated solution generated upon dissolution rapidly crystallizes, or crystallization occurs in the hydrated matrix, the solubility advantage of the amorphous

Table V Comparison Between Different Classification Systems

a Solvent shift (aqueous) *vs*. melt quench (aqueous)

		Solvent shift (aqueous)			Summary	
	%	I	II	III		%
Melt quench (aqueous)	I	26	22	0	Identical	61
	II	4	9	4	Slightly different	37
	III	2	7	26	Extremely different	2

b Solvent shift (aqueous) *vs*. melt quench (solid state)

		Solvent shift (aqueous)			Summary	
	%	I	II	III		%
Melt quench (solid state)	I	26	17	0	Identical	62
	II	6	9	4	Slightly different	38
	III	0	11	28	Extremely different	0

c Solvent shift (aqueous) *vs*. solvent evaporation (solid state)

		Solvent shift (aqueous)			Summary	
	%	I	II	III		%
Solvent evaporation (solid state)	I	20	12	0	Identical	59
	II	7	12	10	Slightly different	41
	III	0	12	27	Extremely different	0

d Melt quench (aqueous) *vs*. melt quench (solid state)

		Melt quench (aqueous)			Summary	
	%	I	II	III		%
Melt quench (solid state)	I	42	4	0	Identical	70
	II	6	4	8	Slightly different	26
	III	4	8	24	Extremely different	4

e Melt quench (aqueous) *vs*. solvent evaporation (solid state)

		Melt quench (aqueous)			Summary	
	%	I	II	III		%
Solvent evaporation (solid state)	I	35	0	0	Identical	70
	II	9	9	12	Slightly different	26
	III	5	5	26	Extremely different	5

formulation will not be realized (7,37). The glass forming ability and glass stability of various compounds has been evaluated previously, both upon cooling APIs from the melt (17,38) and upon rapid evaporation from an organic solvent solution (18). Briefly, using the melt quenching methodology, a Class I compound recrystallizes upon cooling from the melt, a Class II compound does not but does so upon reheating the sample and a Class III shows no crystallization over the timescale of the experiment. For the rapid evaporation approach at least 50% of the sample has crystallized immediately after preparation for a Class I compound and within 7 days for a Class II compound. For a Class III compound, 50% crystallization did not occur within 7 days.

Comparisons between classification results obtained for precipitates suspended in aqueous media, generated using the solvent switch method and those obtained for samples prepared either by melt cooling or rapid solvent evaporation are provided in Table Vb and c, respectively. Both comparisons give very similar results, with about 60% (59–62%) of the compounds being identically classified, 40% (38–41%) being classified slightly different and none of the classifications yielding extremely different results. When comparing the classification results obtained for the melt quenched films exposed to aqueous media with those for samples cooled from the melt (Table Ve) or following rapid solvent evaporation (Table Vf), an even better similarity can be noted, with 70% of the compounds being classified identically. The increased similarity may arise from the fact that the samples are initially prepared as a solid film in all cases in contrast to the solvent switch method where the amorphous precipitates are prepared using a bottom up method (i.e. generated from the solution phase *via* liquid liquid phase separation) (12). In 26% of the cases, slight differences in classification can be observed, and in 4–5% of the cases, extremely different classification results are obtained. These results suggest that a simple evaluation of the crystallization behavior in the solid state, e.g. performed using differential scanning calorimetry (17) or using polarized light microscopy upon rapid solvent evaporation (18) may provide some insight into the type of crystallization behavior that can be expected upon exposure of an amorphous system to an aqueous environment, or into the precipitation outcome from a highly supersaturated solution generated *in vivo* using a supersaturating dosage form.

It is apparent from the results shown in Tables III and IV that the timescales for crystallization in aqueous environments vary dramatically between different compounds. This has obvious implications for understanding behavior *in vivo*. For example, consider the transfer of an initially ionized and solubilized weakly basic compound from the stomach to the small intestine which will result in a decrease in solubility and the generation of supersaturation. For the rapidly crystallizing compounds, it is clear that, in the absence of additives that may delay crystallization, a very short-lived supersaturation period would be expected., It is anticipated that these compounds would have absorption behavior that is more dependent on the equilibrium solubility of the compound, since solution concentration levels will quickly return to these values. In contrast, Class III compounds, which remain non-crystalline for more than an hour, have the potential to form supersaturated solutions that persist for biologically relevant time periods. Class II compounds are likely to be more variable depending on differences in the local environmental conditions and formulation components. Thus the variation in crystallization kinetics seen between the different compounds will likely have a tremendous impact on bioavailability. Based on the experimentally observed differences in crystallization kinetics, it is therefore of great interest to understand what makes a compound a rapid or slow crystallizer. Given the similarity in the crystallization behavior noted for different environments, it is apparent that molecular properties most likely predominantly control crystallization tendency. Previous studies on solid state crystallization behavior from our group using a similar set of model drug compounds, as well as studies from other researchers, have noted that rapid crystallizers tend to have lower molecular weights, fewer rotatable bonds, and a higher thermodynamic driving force for crystallization (17,18,39). Most likely, molecules exhibiting significant conformational flexibility will show a reduced crystallization tendency relative to more rigid molecules (40). It has been demonstrated that compounds that have many competing conformers crystallize less readily (41). Future studies should focus on understanding the factors (especially molecular structure and conformation) that control crystallization kinetics, as well as the extent to which crystallization can be inhibited by additives including endogenous components such as bile salts.. Such studies will lay the foundation for an improved understanding of the role of supersaturated solutions in enhancing bioavailability, as well as contribute to improved *in vitro-in vivo* correlations.

CONCLUSIONS

The crystallization behavior of pharmaceutical molecules in aqueous media was found to be highly dependent on the particular compound studied. While some compounds crystallized almost instantaneously, other systems remained as a hydrated amorphous material for more than an hour. Rapidly crystallizing compounds, formulated as salts, amorphous forms or in other enabling formulations, may show little enhancement in bioavailability if the rapid crystallization kinetics persist *in vivo*. In contrast, poorly water soluble compounds with a persistent hydrated amorphous form have the potential to provide higher biological exposure when formulated as a supersaturating dosage form.

ACKNOWLEDGMENTS AND DISCLOSURES

Use of the Advanced Photon Source was supported by the U. S. Department of Energy, Office of Science, Office of Basic Energy Sciences, under Contract No. DE-AC02- 06CH11357. Dr. Byeongdu Lee and Dr. Xiaobing Zuo (12-ID-B beamline, Advanced Photon Source, Argonne, IL) are acknowledged for their help with the XRPD experiments. B.V.E. is a Postdoctoral Researcher of the "Fonds voor Wetenschappelijk Onderzoek", Flanders, Belgium. The authors would like to thank the National Science Foundation Engineering Research Center for Structured Organic Particulate Systems for financial support (NSF ERC-SOPS)(EEC-0540855).

REFERENCES

1. Lipinski CA. Drug-like properties and the causes of poor solubility and poor permeability. J Pharmacol Toxicol Methods. 2000;44(1): 235–49.
2. Millard JW, Alvarez-Núñez FA, Yalkowsky SH. Solubilization by cosolvents—establishing useful constants for the log-linear model. Int J Pharm. 2002;245(1–2):153–66.
3. Brewster ME, Loftsson T. Cyclodextrins as pharmaceutical solubilizers. Adv Drug Deliv Rev. 2007;59(7):645–66.
4. Stella VJ, Nti-Addae KW. Prodrug strategies to overcome poor water solubility. Adv Drug Deliv Rev. 2007;59(7):677–94.
5. Van Eerdenbrugh B, Van den Mooter G, Augustijns P. Top-down production of drug nanocrystals: nanosuspension stabilization, miniaturization and transformation into solid products. Int J Pharm. 2008;364(1):64–75.
6. Leuner C, Dressman J. Improving drug solubility for oral delivery using solid dispersions. Eur J Pharm Biopharm. 2000;50(1):47–60.
7. Hancock BC, Parks M. What is the true solubility advantage for amorphous pharmaceuticals? Pharm Res. 2000;17(4):397–404.
8. Murdande SB, Pikal MJ, Shanker RM, Bogner RH. Solubility advantage of amorphous pharmaceuticals: I. A thermodynamic analysis. J Pharm Sci. 2010;99(3):1254–64.
9. Murdande SB, Pikal MJ, Shanker RM, Bogner RH. Solubility advantage of amorphous pharmaceuticals: II. Application of quantitative thermodynamic relationships for prediction of solubility enhancement in structurally diverse insoluble pharmaceuticals. Pharm Res. 2010;27(12):2704–14.
10. Murdande SB, Pikal MJ, Shanker RM, Bogner RH. Solubility advantage of amorphous pharmaceuticals, Part 3: Is maximum solubility advantage attainable and sustainable? J Pharm Sci. 2011;100(10): 4349–56.
11. Hsieh YL, Ilevbare GA, Van Eerdenbrugh B, Box KJ, Sanchez-Felix MV, Taylor LS. pH-Induced precipitation behavior of weakly basic compounds: determination of extent and duration of supersaturation using potentiometric titration and correlation to solid state properties. Pharm Res. 2012;29(10):2738–53.
12. Ilevbare GA, Taylor LS. Liquid-liquid phase separation in highly supersaturated aqueous solutions of poorly-water soluble drugs—implications for solubility enhancing formulations. Cryst Growth Des. 2013;13(4):1497–509.
13. Zhou DL, Zhang GGZ, Law D, Grant DJW, Schmitt EA. Physical stability of amorphous pharmaceuticals: importance of configurational thermodynamic quantities and molecular mobility. J Pharm Sci. 2002;91(8):1863–72.
14. Graeser KA, Patterson JE, Zeitler JA, Gordon KC, Rades T. Correlating thermodynamic and kinetic parameters with amorphous stability. Eur J Pharm Sci. 2009;37(3–4):492–8.
15. Van Eerdenbrugh B, Taylor LS. Small scale screening to determine the ability of different polymers to inhibit drug crystallization upon rapid solvent evaporation. Mol Pharm. 2010;7(4):1328–37.
16. Van Eerdenbrugh B, Taylor LS. An *ab initio* polymer selection methodology to prevent crystallization in amorphous solid dispersions by application of crystal engineering principles. CrystEngComm. 2011;13(20):6171–8.
17. Baird JA, Van Eerdenbrugh B, Taylor LS. A classification system to assess the crystallization tendency of organic molecules from undercooled melts. J Pharm Sci. 2010;99(9):3787–806.
18. Van Eerdenbrugh B, Baird JA, Taylor LS. Crystallization tendency of active pharmaceutical ingredients following rapid solvent evaporation—classification and comparison with crystallization tendency from undercooled melts. J Pharm Sci. 2010;99(9):3826–38.
19. Miyajima M, Koshika A, Okada J, Ikeda M, Nishimura K. Effect of polymer crystallinity on papaverine release from poly (L-lactic acid) matrix. J Control Release. 1997;49(2–3):207–15.
20. Van Eerdenbrugh B, Stuyven B, Froyen L, Van Humbeeck J, Martens JA, Augustijns P, *et al*. Downscaling drug nanosuspension production: processing aspects and physicochemical characterization. AAPS PharmSciTech. 2009;10(1):44–53.
21. Van Eerdenbrugh B, Alonzo DE, Taylor LS. Influence of particle size on the ultraviolet spectrum of particulate-containing solutions: implications for *in-situ* concentration monitoring using UV/vis fiber-optic probes. Pharm Res. 2011;28(7):1643–52.
22. Vandecruys R, Peeters J, Verreck G, Brewster ME. Use of a screening method to determine excipients which optimize the extent and stability of supersaturated drug solutions and application of this system to solid formulation design. Int J Pharm. 2007;342(1–2):168–75.
23. Warren DB, Benameur H, Porter CJH, Pouton CW. Using polymeric precipitation inhibitors to improve the absorption of poorly water-soluble drugs: a mechanistic basis for utility. J Drug Target. 2010;18(10):704–31.
24. Bevernage J, Forier T, Brouwers J, Tack J, Annaert P, Augustijns P. Excipient-mediated supersaturation stabilization in human intestinal fluids. Mol Pharm. 2011;8(2):564–70.
25. Alonzo DE, Gao Y, Zhou DL, Mo HP, Zhang GGZ, Taylor LS. Dissolution and precipitation behavior of amorphous solid dispersions. J Pharm Sci. 2011;100(8):3316–31.
26. Brick MC, Palmer HJ, Whitesides TH. Formation of colloidal dispersions of organic materials in aqueous media by solvent shifting. Langmuir. 2003;19(16):6367–80.
27. McMahon LE, Timmins P, Williams AC, York P. Characterization of dihydrates prepared from carbamazepine polymorphs. J Pharm Sci. 1996;85(10):1064–9.
28. Krc J. Crystallographic properties of flufenamic acid. Microscope. 1977;25(1):31–45.
29. McConnell JF. 3′-Trifluoromethyldiphenylamine-2-carboxylic acid, $C_{14}H_{10}F_3NO_2$ flufenamic acid. Cryst Struct Commun. 1973;2:459–61.
30. Allen FH. The Cambridge structural database: a quarter of a million crystal structures and rising. Acta Crystallogr. 2002; B58:380–8.
31. Murthy HMK, Bhat TN, Vijayan M. Structural studies of analgesics and their interactions. 9. Structure of a new crystal form of 2-([3-(trifluoromethyl)phenyl]amino)benzoic acid (flufenamic acid). Acta Crystallogr. 1982;B38:315–7.
32. Chen XM, Li TL, Morris KR, Byrn SR. Crystal packing and chemical reactivity of two polymorphs of flufenamic acid with ammonia. Mol Cryst Liq Cryst. 2002;381:121–31.
33. Mullin JW. Crystallization. 4th ed. Oxford: Elsiever Butterworth-Heinemann; 2001.

34. Peeters J, Neeskens P, Tollenaere JP, Van Remoortere P, Brewster ME. Characterization of the interaction of 2-hydroxypropyl-β-cyclodextrin with itraconazole at pH 2, 4, and 7. J Pharm Sci. 2002;91(6):1414–22.
35. Yalkowsky SH, He Y. Handbook of aqueous solubility data. Boca Raton: CRC Press LLC; 2003.
36. Alonzo DE, Zhang GGZ, Zhou DL, Gao Y, Taylor LS. Understanding the behavior of amorphous pharmaceutical systems during dissolution. Pharm Res. 2010;27(4):608–18.
37. Greco K, Bogner R. Solution-mediated phase transformation: significance during dissolution and implications for bioavailability. J Pharm Sci. 2012;101(9):2996–3018.
38. Baird JA, Thomas LC, Aubuchon SR, Taylor LS. Evaluating the non-isothermal crystallization behavior of organic molecules from the undercooled melt state using rapid heat/cool calorimetry. CrystEngComm. 2013;15(1):111–9.
39. Mahlin D, Ponnambalam S, Hockerfelt MH, Bergstrom CAS. Toward in silico prediction of glass-forming ability from molecular structure alone: a screening tool in early drug development. Mol Pharm. 2011;8(2):498–506.
40. Yu L, Reutzel-Edens SM, Mitchell CA. Crystallization and polymorphism of conformationally flexible molecules: problems, patterns, and strategies. Org Process Res Dev. 2000;4(5):396–402.
41. Hursthouse MB, Huth LS, Threlfall TL. Why do organic compounds crystallise well or badly or ever so slowly? Why is crystallisation nevertheless such a good purification technique? Org Process Res Dev. 2009;13(6):1231–40.